Supporting Information

Deaconescu et al. 10.1073/pnas.1115105109

SI Materials and Methods

Molecular Biology, Protein Expression, and Purification. Transcription-repair coupling factor, TRCF-E730Q and all Cys point mutants (TRCF-A167C, TRCF-H527C, TRCF-A1051C, and TRCF-A1031C) were constructed in the pAD6 plasmid encoding wild-type TRCF by site-directed mutagenesis using the Quikchange kit (Agilent). They were overexpressed and purified as described before (1); where appropriate, gel filtration chromatography was performed immediately before SAXS data collection. Samples were then concentrated and dialyzed against a buffer containing 150 mM NaCl, 20 mM Tris (pH 8.0), 10 mM $MgCl_2$, and 5 mM DTT with and without 5 mM ADP/ATP, respectively. Gel filtration in the absence/presence of nucleotides was performed on a Superdex200 10/300 column (GE Healthcare) by injecting 200 μg TRCF-E730Q and 1 mg TRCFΔ(D1-D3)E730Q and by using buffer conditions identical to those used for SAXS sample preparation. The pAD61 construct encoding TRCFΔ(D1-D3)E730Q (residues 479–1,148 in TRCF) used for SAXS measurements was purified as wild-type TRCF.

The H527C A1031C and A167C G1051C double mutants were created in two Quikchange mutagenesis steps using pAD6 as a template to yield pAD54 and pAD79, respectively, and purified as wild type. No reducing agent was added to buffers used in the purification of TRCF Cys single or double mutants.

For crystallography, the TRCF and UvrA truncations (TRCF-Trunc and UvrA-Trunc, respectively) were generated as follows. Sequences were amplified via PCR using pAD6 and pUNC45 (2) as templates and cloned between the NheI/HindIII sites of a pET28-a derivative to generate pAD36 (encoding residues 127–213 of *Escherichia coli* TRCF) and pAD42 (encoding residues 131–250 of *E. coli* UvrA), respectively. Cultures of transformed Rosetta2 (DE3)pLysS cells were grown to an OD of 0.6 and induced with 1 mM isopropyl-β-D-thiogalactoside at 30 °C for 3 h. For purification, pellets were resuspended in 0.5 M NaCl, 20 mM Tris (pH 8), 5% glycerol, and 2 mM β-mercaptoethanol and purified using Ni^{2+} chromatography as described before (3). After overnight cleavage of the His-tag with Prescission protease, a second subtractive immobilized metal-affinity chromatography step was used to remove the remaining uncleaved recombinant protein. A final gel filtration step on a Sephacryl S-100 column was performed in 100 mM NaCl, 20 mM Tris (pH 8), and 10 mM DTT. For complex assembly, equimolar quantities of TRCF-Trunc and UvrA-Trunc were mixed and incubated on ice.

Pull-Down Assays. For pull-down assays, TRCF derivatives were immobilized to magnetic metal-chelating Dynabeads (Invitrogen) via an N-terminal hexahistidine tag cleavable with Prescission protease (GE Healthcare). Briefly, 250 pmol of purified TRCF-E730Q or TRCF-Trunc were mixed with purified UvrA-Trunc in a 1:4 stoichiometric ratio and incubated for 30 min at room temperature in binding buffer [100 mM NaCl, 20 mM Tris (pH 7.5), 5% glycerol]. Protein sample was then added to equilibrated Dynabeads and incubated for 30 min at 4 °C. Beads were then washed with binding buffer and resuspended in binding buffer supplemented with Prescission protease (GE Healthcare) and 5 mM DTT and further incubated overnight at 4 °C. Beads were then collected on the side of tubes via a magnet, and samples were withdrawn and subjected to SDS/PAGE on 4–12% gels followed by staining with Coomassie Blue.

ATP Binding and ATPase Assays. ATP binding was assayed using photo-cross-linking of radiolabeled ATP to protein. Four micrograms of purified protein was incubated with 10 μM ATP spiked with 5 μCi α-[^{32}P]ATP (3,000 mCi/mmol; Perkin-Elmer) in 150 mM NaCl, 20 mM Tris (pH 8), 1 mM DTT, and 5% glycerol in a reaction volume of 20 μL without/with the indicated amount of competitor ATP for 15 min at 20 °C. Samples were then placed as small drops on cooled parafilm-wrapped microscope slides on ice and irradiated at 254 nm in a Stratalinker 1800 UV source for 2 min (0.24 J/cm^2). Samples were then mixed with SDS loading buffer, boiled, and run on 4–16% Bis-Tris SDS/PAGE (Invitrogen). Gels were stained for protein with Coomassie Blue and exposed using a phosphor storage screen.

ATPase assays were carried out in triplicate at 25 °C using the EnzCheck Phosphate Assay kit (Molecular Probes) with a buffer consisting of 100 mM NaCl, 50 mM Hepes (pH 7.4), 10 mM $MgCl_2$, 5% glycerol, and 5 mM ATP at protein concentrations ranging from 0.5 to 4 μM. Turnover numbers were obtained by fitting the linear portion of the curves using regression analysis and calculating the slope of the linear fit with the kinetics module of Swift II software (Biochrome).

Stimulated ATPase Assays. For testing the effects of ternary elongation complexes (TECs) on ATP turnover by TRCF, stalled TECs were prepared by nucleotide starvation as for RNA polymerase (RNAP) release assays. Briefly, 600 nM TECs (or naked ~150-bp dsDNA template) was mixed with 0.25 mM cold ATP spiked with 10 μCi of γ-[^{32}P]ATP, followed by addition of 800 nM TRCF at time 0. Reactions were then incubated at 37 °C for 2, 5, and 10 min and quenched by addition of an equal volume (2 μL) of acetic acid. A total of 0.4 μL of the mixture was analyzed by thin layer chromatography on polyethylenimine cellulose plates (Sigma), which were developed in 750 mM KH_2PO_4 (pH 3.5). Released $^{32}P_i$ was visualized and quantified by phosphorimaging. The reported percentage of Pi released was calculated according to the following relationship:

$$\%\ \text{of}\ P_i = P_i\ \text{intensity} * 100/\text{total signal in the relevant lane (corresponding to both hot ATP and hot}\ P_i).$$

Design and Biochemical Studies of Disulfide-Locked Mutants. For rational design of disulfide bonds that would restrain D7, we have used Disulfide by Design (4), a software package that, given a protein structure coordinate file [e.g., Protein Data Bank (PDB) ID 2EYQ], computes all possible proximal residue pairs with a geometry consistent with the geometry of a disulfide bond. This allowed us to identify H527 and A1031 as good candidate substitutions. However, this in silico tool did not predict any suitable residue pair that would tether D2 to D7 (and would prevent exposure of the UvrA-binding surface). We have thus proceeded to design the TRCF-D2:D7 mutant strictly on the basis of spatial proximity considerations by inspection of the crystal structure of nucleotide-free TRCF. We underscore that, in both TRCF-D2:RID and TRCF-D2:D7, some movements of the cross-linked domains may still be accommodated.

For cross-linking studies, protein was first reduced by incubation with 20 mM tris(2-carboxyethyl)phosphine on ice for 1 h, and buffer was subsequently exchanged to 0.1 M NaCl, 50 mM Hepes (pH 7.0), and 10 mM $MgCl_2$ with/without 5 mM ADP or ATPγS. Oxidative disulfide cross-linking reactions were carried out in the presence of a phenanthroline (CuPh) catalyst at the indicated concentrations for 10 min at room temperature and quenched with 50 mM iodoacetamide and SDS loading buffer supplemented with 50 mM EDTA in order to chelate the cupric

ions. SDS/PAGE page was carried out on 3–8% Tris-acetate gels (Invitrogen) under standard nonreducing or reducing conditions.

For cross-linking studies in the presence of UvrA-Trunc, a CuPh concentration of 4 μM was used with 4 μg of TRCF mutant and increasing concentrations of purified UvrA-Trunc in a buffer consisting of 100 mM NaCl, 20 mM Tris (pH 7.5), 10 mM $MgCl_2$, and 5% glycerol. The TRCF-D2:D7:UvrA-Trunc stoichiometry of the reactions shown in Fig. 2 were 2:1, 1:3, 1:5, and 1:10. Reactions were carried out for 10 min at room temperature and were terminated and analyzed as above. Densitometry was carried out using the Kodak-1D software. We note the weak staining of UvrA-Trunc, which is much smaller than full-length TRCF (~13 versus 130 kDa). Under the electrophoresis conditions required for optimum separation of reduced from oxidized species, UvrA-Trunc migration overlaps with the dye front, making its visualization more difficult as in Fig. 4*D*. Under a shorter electrophoresis run time, UvrA-Trunc can be clearly visualized (Fig. 4*D*, lane 10). For CuPh-catalyzed oxidation of TRCF-D2:RID (Fig. S3*C*), uncleaved UvrA-Trunc carrying an N-terminal hexahistidine tag was used.

For cross-linking of TRCF variants in the presence of dsDNA, we have used the same 90-bp dsDNA fragment and buffer system used in our fluorescence anisotropy assays. Protein and DNA were mixed in the stoichiometric ratios indicated in Fig. S7*C* (from 4:1–1:3 of TRCF variant:DNA). Oxidation was initiated by addition of 10 μM CuPh (for TRCF-D2:D7) and 4 μM CuPh (for TRCF-D2:RID) and stopped as described above, and samples were subjected to nonreducing SDS/PAGE on 3–8% Tris-acetate gels. DNA integrity was also assessed using 5% agarose electrophoresis and ethidium bromide staining. White shadow immediately above the DNA bands in Fig. S7*D* is due to the tracking dye. Cuprous ions and phenanthroline are known to form a chemical nuclease (5) that can fragment the DNA present in the oxidation reactions. In the presence of reducing agent, cupric ions and phenanthroline could potentially be converted to chemical nuclease, degrading the DNA and confounding the assays. Although no reducing agent was added in the buffer used for these oxidation reactions, carryover of reducing agent from the previous experimental step (the complete reduction of the Cys variants and buffer exchange) represents a concern. However, agarose electrophoresis indicates that DNA is not affected under experimental conditions.

Size-exclusion chromatography of TRCF-D2:RID/TRCF-D2:D7 and TRCF was carried out on a Superdex 200 10/300 gel filtration column (GE Healthcare) run in a buffer consisting of 0.25 M NaCl, 20 mM Tris (pH 8), 5% glycerol, and no reducing agent. For calibration purposes, a gel filtration calibrant kit (Bio-Rad) was used in conjunction with purified catalase from *Aspergillus niger* (Sigma Aldrich), which provides a standard of a molecular weight (250 kDa) similar to the theoretical molecular weight of a putative TRCF dimer (260 kDa).

Fluorescence Anisotropy Assays. A double-stranded 90-bp DNA fragment was generated by conventional PCR amplification with flanking primers, one of which contains a HEX fluorophore at the 5′ end, and the product was further purified using conventional agarose gel purification methods. Fluorescently labeled DNA (20 nM) was titrated with increasing concentrations of wild-type TRCF or TRCF-E730Q. DNA was added into 1.5 mL of buffer containing 20 mM Hepes (pH 7.5), 50 mM NaCl, and 2 mM β-mercaptoethanol, with or without 2 mM ATPγS (Merck), as indicated. To assess binding by TRCF-D2:D7, titrations were performed with oxidized protein in 20 mM Hepes (pH 7.5), 50 mM NaCl, and 2 mM ATPγS without DTT. Reduced TRCF-D2:D7 was also assayed under a similar buffer system, which included 4 mM DTT. After the addition of TRCF variants, the reaction was equilibrated for 5 min at 25 °C before measurements were recorded. Fluorescence anisotropy was measured at 555 nm using a F-7000 fluorescence spectrophotometer (Hitachi). The K_d values were calculated from three independent experiments using the Micromath Scientist software package.

DNaseI Footprinting Assays. Footprinting assays used a template containing the T7A1 promoter and a 147-nt G-less initial transcribed region, which was generated by PCR amplification using the pRL596 plasmid. The nontemplate DNA strand primer was end-labeled with [P^{32}]-γATP (Perkin-Elmer) using polynucleotide kinase from Epicentre and purified using G-50 spin columns (GE Healthcare). PCR products were gel-purified using a gel purification kit (Promega). The halted C147 TECs were assembled at 37 °C for 20 min with 20 nM of labeled DNA fragment; 400 nM wild-type holo *E. coli* RNAP; 25 μM ATP, GTP, and CTP; and 100 μM ApU in transcription buffer (44 mM Tris·HCl, 14 mM $MgCl_2$, 20 mM NaCl, 5% glycerol, 0.1 mM EDTA, pH 7.9). Then ATPγS was added to 2 mM, and TRCF variants were added to 120 nM (wild type and TRCF-D2:D7) or 250 nM (TRCF-E730Q). After 2 min of incubation, complexes were treated with 0.15 units of DNaseI (Epicentre) for 1 min, and digestions were then quenched by the addition of an equal volume of phenol. Samples were subjected to phenol-chloroform extraction and precipitated with ethanol. Pellets were then dissolved in 96% formamide, heated at 95 °C for 3 min, and analyzed on 7 M urea, 8% (wt/vol) acrylamide:bisacrylamide (19:1) denaturing gels. To determine footprint boundaries, a dideoxy sequencing ladder using labeled primer was generated with a SequiTherm kit (Epicentre). As controls, digestion reactions were carried out in the absence of added proteins or in the presence of TRCF alone (without RNAP, but with all other components). The boundaries of C^{147} in the absence or in the presence of TRCF were established using trace analysis with the trace obtained in the absence of proteins as a baseline (black in Fig. S2*F*). In the halted TEC, positions from −14 to +15 (relative to the active site of RNAP) are protected against DNaseI cleavage, consistent with the results obtained under the same conditions with other defined TECs (6). TRCF binds specifically to the TEC, extending the upstream boundary of DNA protection from 14 to 39 bp. All TRCF variants bound efficiently to the halted TEC despite their differences in affinity to naked DNA and the efficiency of RNA release observed in the experiments described above. Under these reaction conditions, no specific DNA protection by TRCF was observed in the absence of RNAP.

RNA Release Assays. RNA release assays were carried out with modifications using a previously published protocol (7), and used a template derived from a previously described plasmid, pIA226 (8), containing the phage λ P_R promoter followed by a C-less transcribed region. This transcription template was prepared by PCR amplification with flanking primers, one of which contained a triethylene-glycol-coupled biotin (TEG-biotin) moiety at its 5′ end. [α^{32}P]-labeled halted A26 TEC was formed by CTP deprivation in TGA10 buffer (20 mM Tris-acetate, 20 mM Na acetate, 10 mM Mg acetate, 1 mM DTT, 0.1 mM EDTA, 5% glycerol, pH 7.9) and immobilized on streptavidin-coated magnetic beads (DynaBeads T1, Invitrogen). Beads were washed three times with 1 mL of the reaction buffer (TGA10 without DTT) containing 200 mM NaCl to remove abortive RNA products and any residual reducing agent and incubated with TRCF (at 40 or 4 nM final concentration) at 37 °C for 1 min. Reactions were initiated by addition of 2 mM ATP, and RNA released into the supernatant was removed at various time points, mixed with an equal volume of 2× STOP solution [10 M urea, 50 mM EDTA, 45 mM Tris-borate (pH 8.3), 0.1% bromophenol blue, 0.1% xylene cyanol], and loaded onto a 10% denaturing urea-acrylamide (19:1) gel in a buffer consisting of 45 mM Tris, 45 mM boric acid, 1 mM EDTA.

The ability of the cross-linked TRCF-D2:D7 variant to dissociate TECs (Fig. 4*B*) could be explained if the disulfide bond in this variant were reduced under the conditions of the RNA release, e.g., due to the presence of an unidentified reducing agent not removable by washing of the beads. Formation of the disulfide bridge between Cys167 and Cys1051 substantially alters the mobility of TRCF-D2:D7, allowing us to evaluate this possibility directly. We assembled mock reactions on three different types of DynaBeads beads (A–C, where B was the batch used for the RNA release assays) under the conditions similar to those in Fig. 4*B*, except that (*i*) the ^{32}P-labeled GTP was omitted and (*ii*) TRCF-D2:D7^{ox} protein was present at 500 nM to allow for in-gel detection. As a control, TRCF-D2:D7^{ox} alone was treated with DTT at the indicated concentrations. The reactions were incubated at 37 °C for 16 min (the longest incubation time used in the release assays), stopped, and loaded onto a 3–8% Tris-acetate gel, as shown in Fig. S3*B*. There was no evidence for reduction of the D2–D7 disulfide due to the magnetic beads used.

Limited Proteolysis. Limited proteolysis of TRCF in the absence and presence of the nucleotides ADP and ATPγS/ATP was carried out using trypsin, chymotrypsin, and subtilisin (Sigma-Aldrich). Protein (25 μg) was mixed with decreasing concentrations of protease at 1:1, 1:10, 1:100, and 1:1,000 protease-to-protein molar ratio and incubated at room temperature for 30 min. Reactions were carried out in a buffer consisting of 100 mM NaCl, 20 mM Tris (pH 8.0), and 10 mM $MgCl_2$ (with and without 5 mM ADP and ATPγS, respectively) and stopped by the addition of 10 mM PMSF and SDS-loading buffer. Samples were subsequently analyzed by SDS/PAGE on 4–12% Bis-Tris gels stained with Coomassie Blue.

Structure Solution and Crystallographic Refinement. For determining the structure of the TRCF–Trunc/UvrA–Trunc complex, data were indexed, reduced, and scaled, and phases were obtained using molecular replacement with Phaser (9). To generate a search model, D2 of *E. coli* TRCF (PDB ID 2EYQ) was superimposed onto the homologous domain of *Geobacillus stearothermophilus* UvrB in the UvrA–UvrB complex structure (PDB ID 3FPN), and then the resulting hybrid model was edited on the basis of a pairwise sequence alignment. Coordinates were subsequently refined using iterative cycles of manual building in Coot (10) and PHENIX refinement (11) The final model has no residues in the disallowed region of the Ramachandran plot as assessed using MolProbity. A section of the sigmaA $2|F_o| - |F_c|$ map is presented in Fig. S8*B*.

SAXS Data Collection and Processing. Data were collected using a detector distance of 1,475 mm and a radiation energy of 12 keV. The buffer consisted of 150 mM NaCl, 20 mM Tris (pH 8), 5 mM DTT, 10 mM $MgCl_2$, and nucleotide at 5 mM, if any, for full-length TRCF, and 250 mM NaCl, 20 mM Tris (pH 8), 10 mM $MgCl_2$, 1% glycerol, and 5 mM DTT with/without 2 mM ADP/ATP for the truncated TRCF variant. Samples and matching buffer were exposed for 0.5 and 5 s for full-length TRCF-E730Q and for 1 and 10 s for TRCFΔ(D1-D3)E730Q, respectively. A second 0.5-s/1-s exposure was recorded after the long exposure to assess radiation damage, which was minimal. Raw scattering data were azimuthally averaged and normalized, and buffer scattering was subtracted using the resident software of the Sibyls beamline. Individual scattering curves for a given state that were collected at different concentrations or exposure duration were merged together using PRIMUS (12) to yield a low-noise interference-free composite curve. Guinier plot analysis was used to assess any potential aggregation, which was not present at protein concentrations less than 4 mg/mL. Radii of gyration were initially computed on the basis of the Guinier plot analysis in PRIMUS (Fig. S8*A*) using data points satisfying the requirement $qR_g < 1.3$ (where q represents momentum transfer and R_g the radius of gyration) and subsequently using the second moment of the pair distribution function. Pair distribution function [$p(r)$] and maximum intramolecular distance (D_{max}) values were calculated using the indirect Fourier transform as implemented in GNOM. To properly assess D_{max}, $p(r)$ was initially not constrained to be zero at D_{max}. This gave us an initial estimate of D_{max} that was used in subsequent analysis. For the final processing of the data, $p(r)$ was constrained to become zero at D_{max}. Good agreement was found between the radii of gyration calculated from the second moment of $p(r)$ compared with the values derived from the Guinier plot (Fig. S8*A*) and shown in Table S2.

Modeling of SAXS Data. Ab initio simulations were performed using GASBOR (13) with structure minimization being carried out against the composite, merged scattering curve rather than the pair distribution function $p(r)$. Fifteen independent simulations were performed for each of the nucleotide-free, ADP-, and ATP-bound TRCF datasets. Sets of simulations were carried out at several r_{max} values to ensure the absence of any artifactual boundary effects resulting from using too small a search volume. The mean χ for the resulting models were 1.4 ± 0.2 for nucleotide-free; 1.4 ± 0.1 for ADP-bound; 1.2 ± 0.07 ATP-bound full-length TRCF; 1.1 ± 0.03 for TRCFΔ(D1-D3); 1.4 ± 0.05 for ADP-bound; and 1.5 ± 0.05 for ATP-bound TRCFΔ(D1-D3). Resulting models were then aligned, averaged, and filtered using the DAMAVER and DAMFILT packages (14). The criterion for including the models in the averaging process was normalized spatial discrepancy (NSD) < mean NSD + 2* variation, where NSD is calculated with SUBCOMP (14) during the initial alignment of the models. According to this criterion, one simulation was discarded for nucleotide-free TRCF-E730Q and TRCFΔ(D1-D3)E730Q, and all 15 simulations were used for all of the other protein samples. The average NSD values for our simulations were as follows: 1.41 ± 0.05 (TRCF-E730Q), 1.45 ± 0.03 (ADP-bound TRCF-E730Q), 1.48 ± 0.04 (ATP-bound TRCF-E730Q), 1.37 ± 0.06 [TRCFΔ(D1-D3)E730Q], 1.24 ± 0.03 [ADP-bound TRCFΔ(D1-D3)E730Q], and 1.26 ± 0.04 [ATP-bound TRCFΔ(D1-D3)E730Q].

We also carried out simulations of the nucleotide-free TRCF using the coordinates of the Cα backbone of apo *E. coli* TRCF (PDB ID 2EYQ) as input in GASBOR. These simulations converged with similar NSD, but with a slightly higher discrepancy against the raw data, suggesting that seeding the search with the crystal structure coordinates may have trapped the simulation in a local minimum. Therefore, in order to avoid bias, we used only the ab initio nucleotide-free model for analysis. The crystallographic TRCF model was docked as a rigid body using the colores module of SITUS (15) to carry out an exhaustive search and then was locally refined in Chimera (16). Our data did not allow us to generate a physically consistent pseudoatomic model for ADP/ATP-bound TRCF through combined rigid-body fitting of individual domains and combined SAXS/molecular dynamics methods, likely due to the large number of moving domains as well as the presence of multiple interlocking structural elements that are believed to move upon nucleotide binding (namely the TRG motif, hook helices, relay helix, and multiple interdomain loops seen in Fig. 1*A*). We therefore attempted to place the available crystal structure of nucleotide-free TRCF in the SAXS envelope of ATP-bound TRCF using rigid-body fitting with SITUS and Chimera (15, 16). We obtained two distinct fitting solutions resulting in equally poor cross-correlation (Fig. S6*C*).

1. Deaconescu AM, Darst SA (2005) Crystallization and preliminary structure determination of Escherichia coli Mfd, the transcription-repair coupling factor. *Acta Crystallogr Sect F Struct Biol Cryst Commun* 61:1062–1064.
2. Thomas DC, Levy M, Sancar A (1985) Amplification and purification of UvrA, UvrB, and UvrC proteins of Escherichia coli. *J Biol Chem* 260:9875–9883.
3. Deaconescu AM, et al. (2002) X-ray structure of Saccharomyces cerevisiae homologous mitochondrial matrix factor 1 (Hmf1). *Proteins* 48:431–436.
4. Dombkowski AA (2003) Disulfide by Design: A computational method for the rational design of disulfide bonds in proteins. *Bioinformatics* 19:1852–1853.
5. Sigman DS, Graham DR, D'Aurora V, Stern AM (1979) Oxygen-dependent cleavage of DNA by the 1,10-phenanthroline cuprous complex. Inhibition of Escherichia coli DNA polymerase I. *J Biol Chem* 254:12269–12272.
6. Krummel B, Chamberlin MJ (1992) Structural analysis of ternary complexes of Escherichia coli RNA polymerase. Deoxyribonuclease I footprinting of defined complexes. *J Mol Biol* 225:239–250.
7. Park J-S, Marr MT, Roberts JW (2002) *E. coli* transcription repair coupling factor (Mfd protein) rescues arrested complexes by promoting forward translocation. *Cell* 109: 757–767.
8. Artsimovitch I, Landick R (2000) Pausing by bacterial RNA polymerase is mediated by mechanistically distinct classes of signals. *Proc Natl Acad Sci USA* 97:7090–7095.
9. McCoy AJ, et al. (2007) Phaser crystallographic software. *J Appl Cryst* 40:658–674.
10. Emsley P, Cowtan K (2004) Coot: model-building tools for molecular graphics. *Acta Crystallogr D Biol Crystallogr* 60(Pt 12 Pt 1):2126–2132.
11. Adams PD, et al. (2002) PHENIX: building new software for automated crystallographic structure determination. *Acta Crystallogr D Biol Crystallogr* 58:1948–1954.
12. Konarev PV, Volkov VV, Sokolova AV, Koch MHJ, Svergun DI, Koch HJ (2003) PRIMUS: A Windows PC-based system for small-angle scattering data analysis. *J Appl Cryst* 36: 1277–1282.
13. Svergun DI, Petoukhov MV, Koch MH (2001) Determination of domain structure of proteins from X-ray solution scattering. *Biophys J* 80:2946–2953.
14. Volkov V, Svergun DI (2003) Uniqueness of ab initio shape determination in small-angle scattering. *Biophys J* 80:2946–2953.
15. Wriggers W, Birmanns S (2001) Using situs for flexible and rigid-body fitting of multiresolution single-molecule data. *J Struct Biol* 133:193–202.
16. Pettersen EF, et al. (2004) UCSF Chimera: A visualization system for exploratory research and analysis. *J Comput Chem* 25:1605–1612.

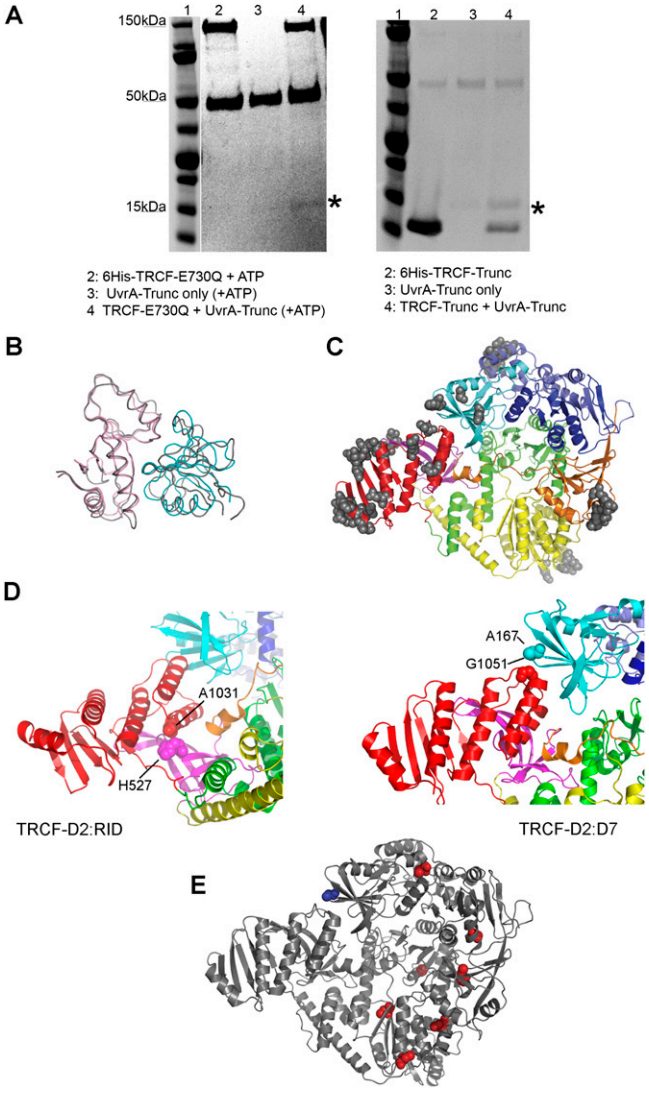

Fig. S1. TRCF and UvrB share a similar mode of binding to UvrA. (*A*) Pull-down assays demonstrating binding of UvrA-Trunc to TRCF derivatives. Complexes were immobilized via a hexahistine tag on TRCF-E730Q (*Left*, in the presence of 5 mM ATPγS) and TRCF-Trunc (*Right*) and then released after washing of the beads via cleavage of the His-tag with Prescission protease. Asterisks indicate bands of pulled-down UvrA-Trunc. Bands migrating near the 50-kDa marker constitute Prescission protease. (*B*) Worm representation of TRCF-Trunc/UvrA-Trunc and the core UvrB/UvrA complex superposed on the Cα atoms of the UvrA domain (root-mean-square displacement of 1.3 Å). TRCF-Trunc is colored in cyan, and UvrA-Trunc and the interacting UvrB domain are shown in pink and gray, respectively. We note in this superposition a small relative rotation of TRCF-Trunc and the UvrB domain relative to the UvrA domain, resulting in a 1.8-Å distance between the centroids of TRCF-Trunc and the UvrB domain. (*C*) TRCF color-coded by domain as in Fig. 1 with residues involved in crystal packing shown as gray spheres. (*D*) Close-up view of domains tethered via disulfide cross-links engineered using Cys substitutions at strategic positions (indicated by spheres) within D2 and RID (TRCF-D2:RID) and D2 and D7 (TRCF-D2:D7). Domains are colored using the coloring scheme of Fig. 1. (*E*) Ribbon representation of TRCF with cysteine residues shown as red spheres and the engineered C167 as blue spheres.

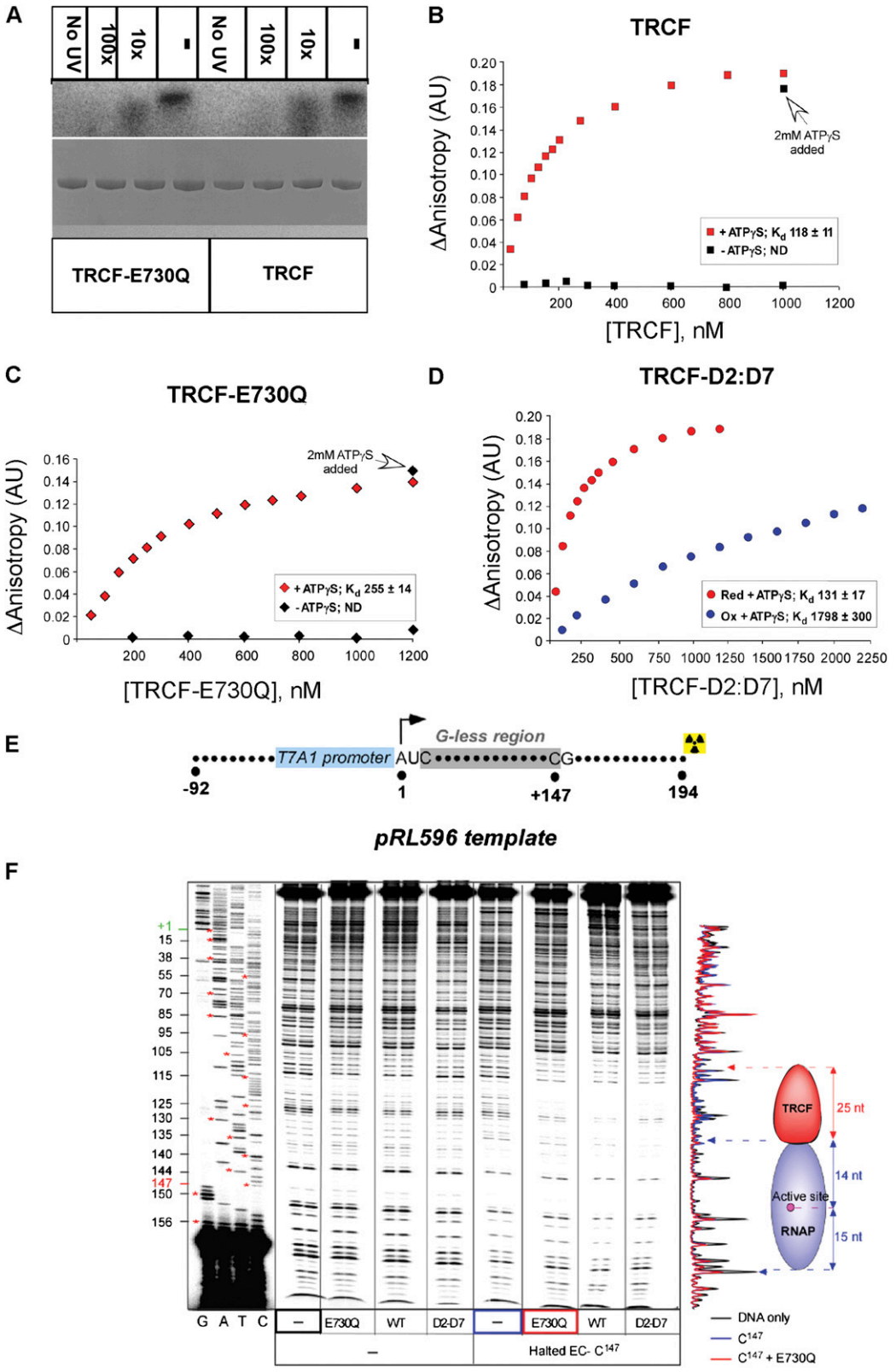

Fig. S2. Biochemical characterization of TRCF variants. (*A*) SDS/PAGE of ATP cross-linked to TRCF and TRCF-E730Q stained with Coomassie Blue (*Lower*) or exposed in a phosphor storage screen (*Upper*). (*B–D*) Representative binding isotherms showing the binding of TRCF variants to a HEX-labeled dsDNA fragment. The units of the determined K_d values are indicated in nanomolar. In control experiments lacking ATP (black symbols), the last sample was measured before and after (as indicated by arrows) the addition of 2 mM ATPγS. Titrations were performed in triplicate with wild-type TRCF (*B*), TRCF-D2:D7 protein both without (blue symbols) or with (red symbols) 4 mM DTT (*D*), as well as the TRCF-E730Q mutant (*C*). (*E*) Schematic representation of the transcription template containing a T7A1 promoter used for generating halted TECs for TRCF binding. Nucleotide positions are indicated in numbers relative to the transcription start site labeled "1." (*F*) Representative denaturing PAGE of the DNaseI digestion reactions (*Right*, loaded in duplicate) as well as the dideoxy sequencing ladder

Legend continued on following page

(*Left*, labeled GATC) used for mapping the binding site of wild-type TRCF, TRCF-E730Q, and oxidized TRCF-D2:D7 (in the D2–D7-labeled lanes) relative to the halted TEC. Numbers on the left of the sequencing ladder mark positions from the transcription start site (corresponding bands are indicated by the asterisks on the gel). As a control, digestion reactions were carried out in the absence of added proteins (the leftmost panel) or in the presence of TRCF alone. The boundaries of C^{147} in the absence (blue) or in the presence of TRCF (red) were established using trace analysis. Digestion of the DNA in the absence of proteins was used as a baseline. In the halted TEC, positions from −14 to +15 [relative to the RNA polymerase (RNAP) active site] are protected against DNaseI cleavage, consistent with results obtained under the same conditions with other defined TECs (6). TRCF binds specifically to the TEC, extending the upstream boundary of DNA protection from 14 to 39 bp. TRCF variants bound efficiently to the halted TEC despite their differences in affinity to the naked DNA and the efficiency of RNA release observed in the experiments described here. Under these reaction conditions, no specific DNA protection by TRCF was observed in the absence of RNAP.

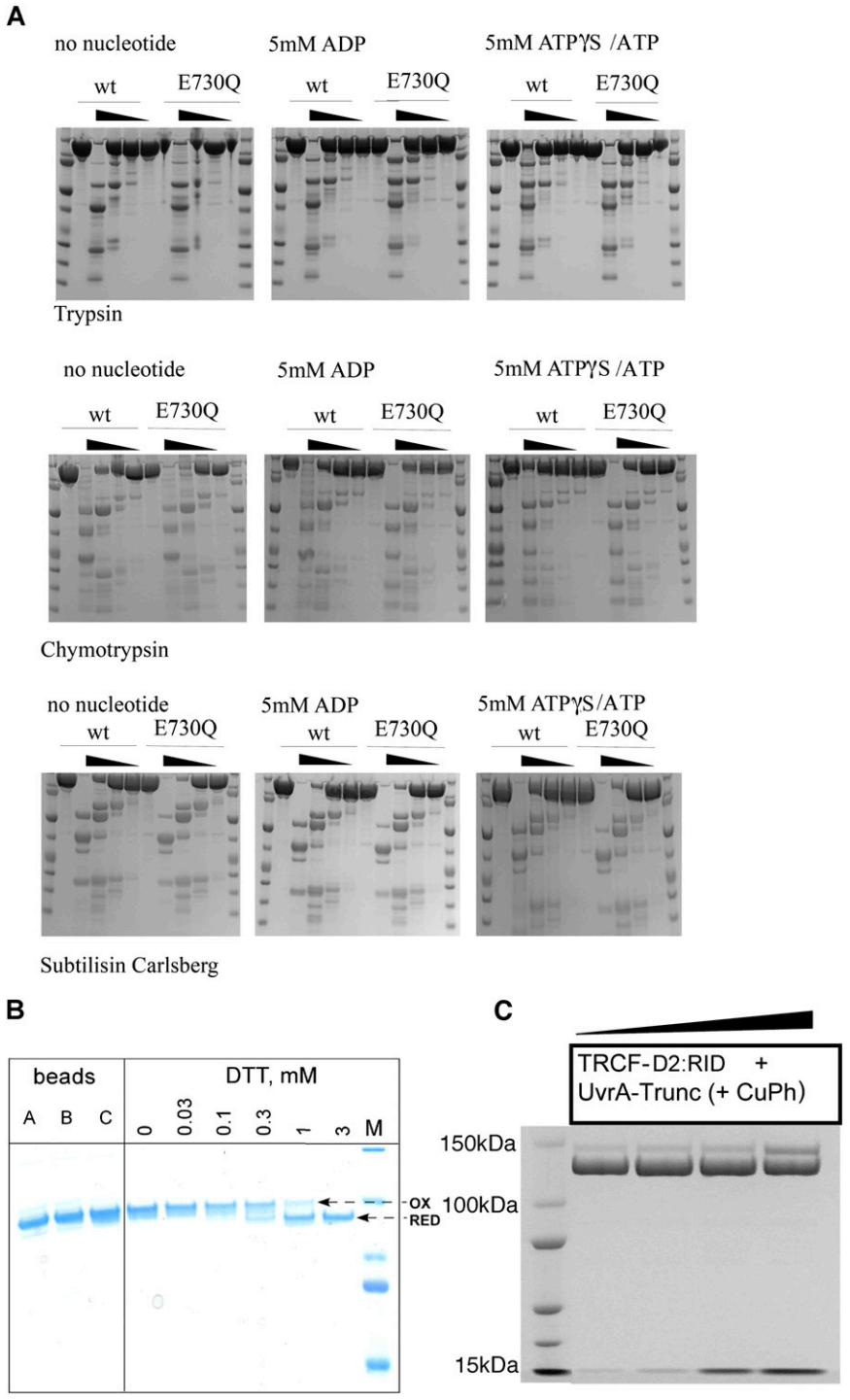

Fig. S3. Limited proteolysis of TRCF and TRCF-E730Q and cross-linking of TRCF variants. (*A*) Digestions were carried out with increasing concentrations of trypsin (*Top*), chymotrypsin (*Middle*), and subtilisin Carlsberg (*Bottom*). (*B*) SDS/PAGE of the TRCF-D2:D7 variant after incubations with the magnetic beads used in RNA-release assays and increasing concentrations of reducing agents. (*C*) SDS/PAGE of TRCF-D2:RID oxidized in the presence of 4 μM Cu(II) (1, 10) phenanthroline (CuPh) and increasing concentrations of UvrA-Trunc.

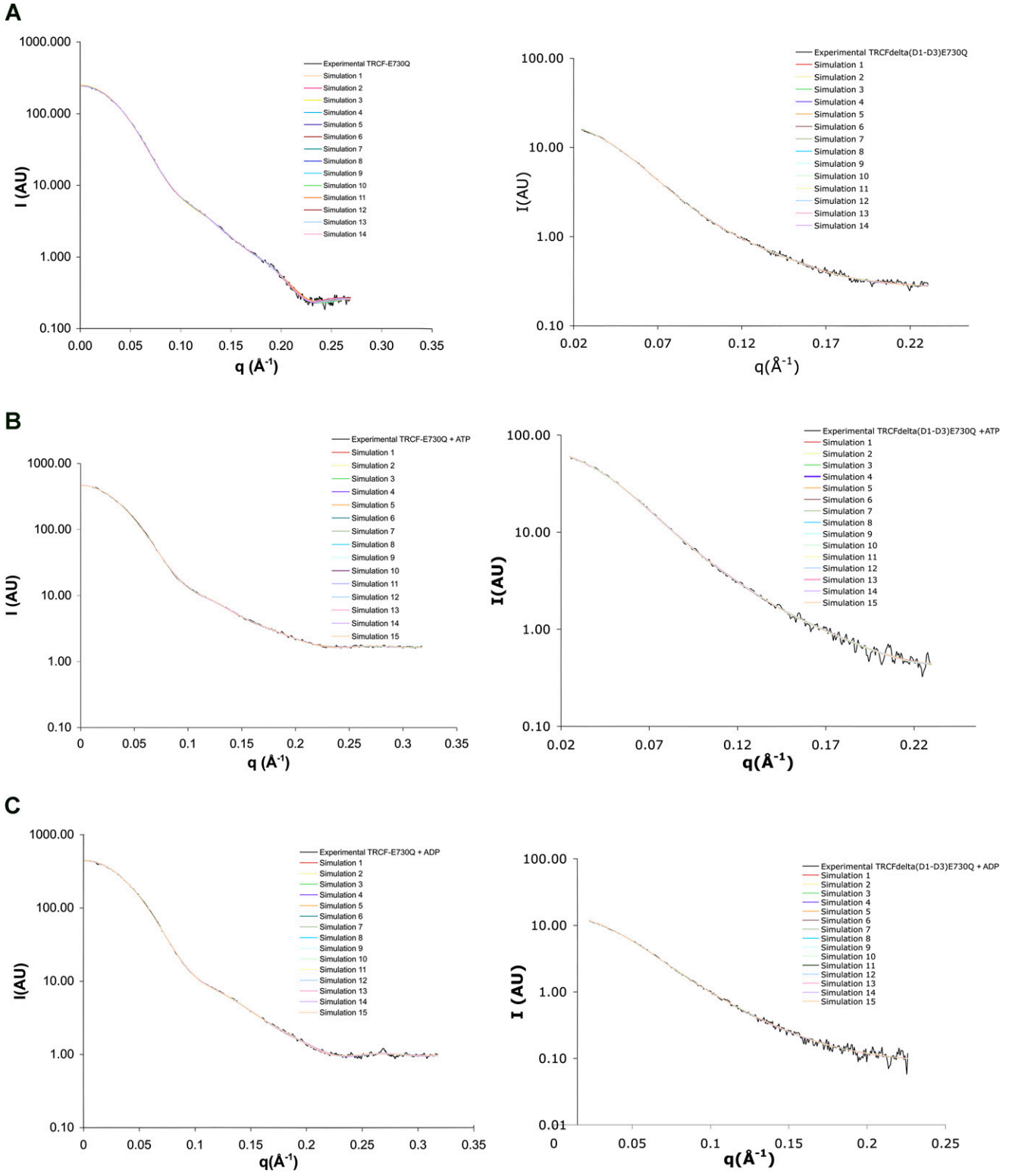

Fig. S4. Comparison between the observed and simulated scattering of the obtained GASBOR dummy residue models obtained in the absence of nucleotide (*A*), with ATP (*B*) and ADP (*C*).

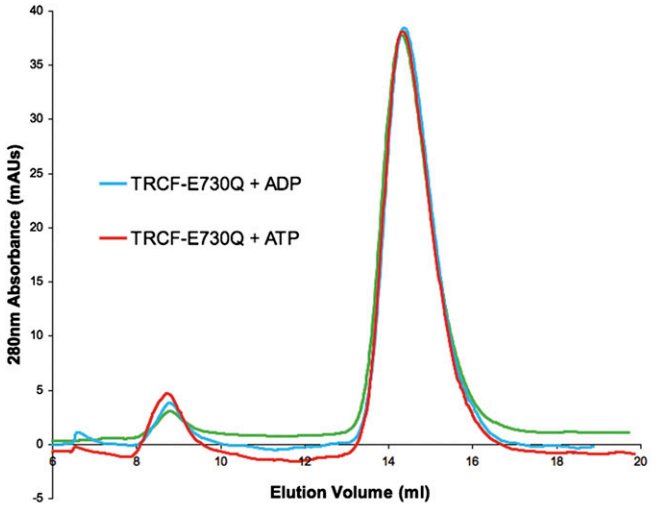

Theoretical Molecular Weight: 130 kDa
Apparent Molecular Weight :
TRCF-E730Q: 130 kDa
TRCF-E730Q + ADP: 130 kDa
TRCF-E730Q + ATP: 130 kDa

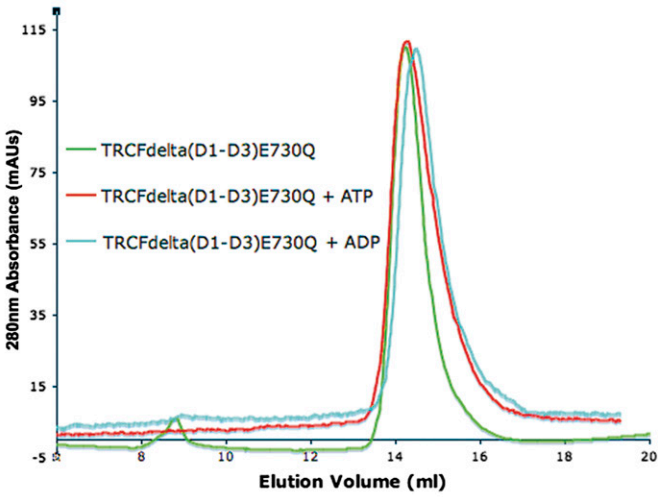

Theoretical Molecular Weight: 76 kDa
Apparent Molecular Weight:
TRCFdelta(D1-D3)E730Q: 73 kDa
TRCFdelta(D1-D3)E730Q + ADP: 64 kDa
TRCFdelta(D1-D3)E730Q + ATP: 70 kDa

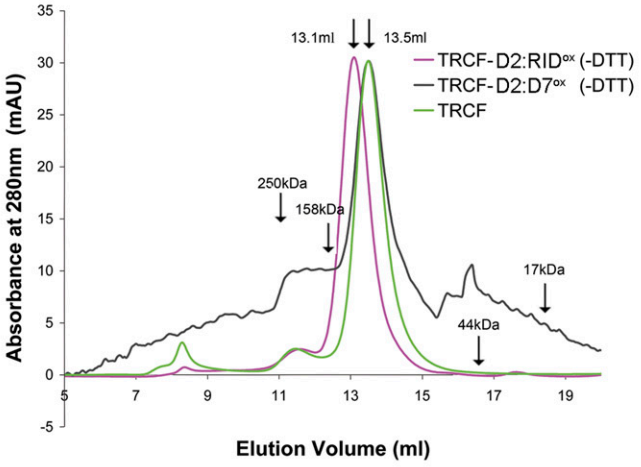

TRCF Apparent Molecular Weight = 124kDa
TRCF-D2:RIDox Apparent Molecular Weight= 148kDa
TRCF-D2:D7ox Apparent Molecular Weight= 124kDa

Fig. S5. Size-exclusion chromatography confirms TRCF variants are monomeric. Curves indicate the elution of TRCF-E730Q and TRCF-E730QΔ(D1-D3)E730Q in the absence of nucleotide (green), with ADP (cyan) or ATP (red). *Lower* panel indicates the elution profile of oxidized TRCF variants, demonstrating the engineered disulfides are intramolecular rather than intermolecular.

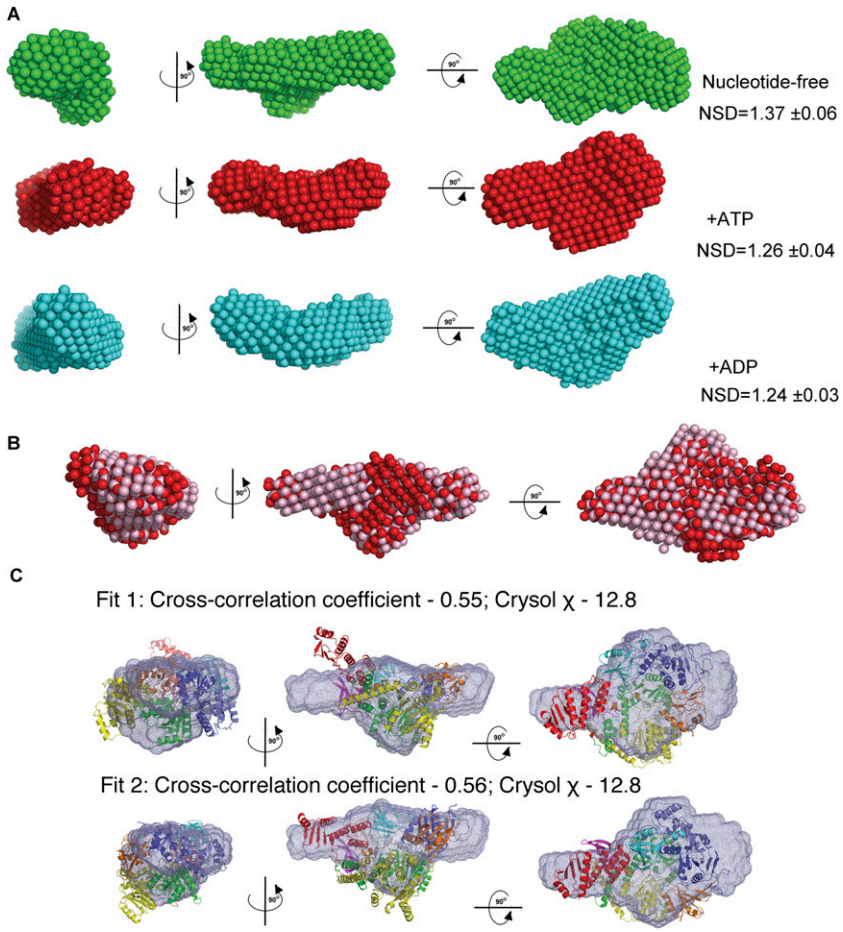

Fig. S6. SAXS bead models. (*A*) Models for the hyperactive variant TRCFΔ(D1-D3)E730Q. (*B*) Ab initio (red) and coordinate-seeded model (pink) for ATP-bound TRCF. Views are as in Fig. 3, and mean NSD values are indicated with SD. (*C*) Rigid-body fitting of the crystallographic model of nucleotide-free TRCF into the SAXS envelopes obtained for the TRCF-E730Q mutant in the presence of ATP. Fitting of the atomic model into the SAXS-derived volumetric map resulted in two possible placements with a similar correlation coefficient. The X-ray TRCF model is color-coded by domain as in Fig. 1, and the SAXS volumetric map is represented as a gray mesh.

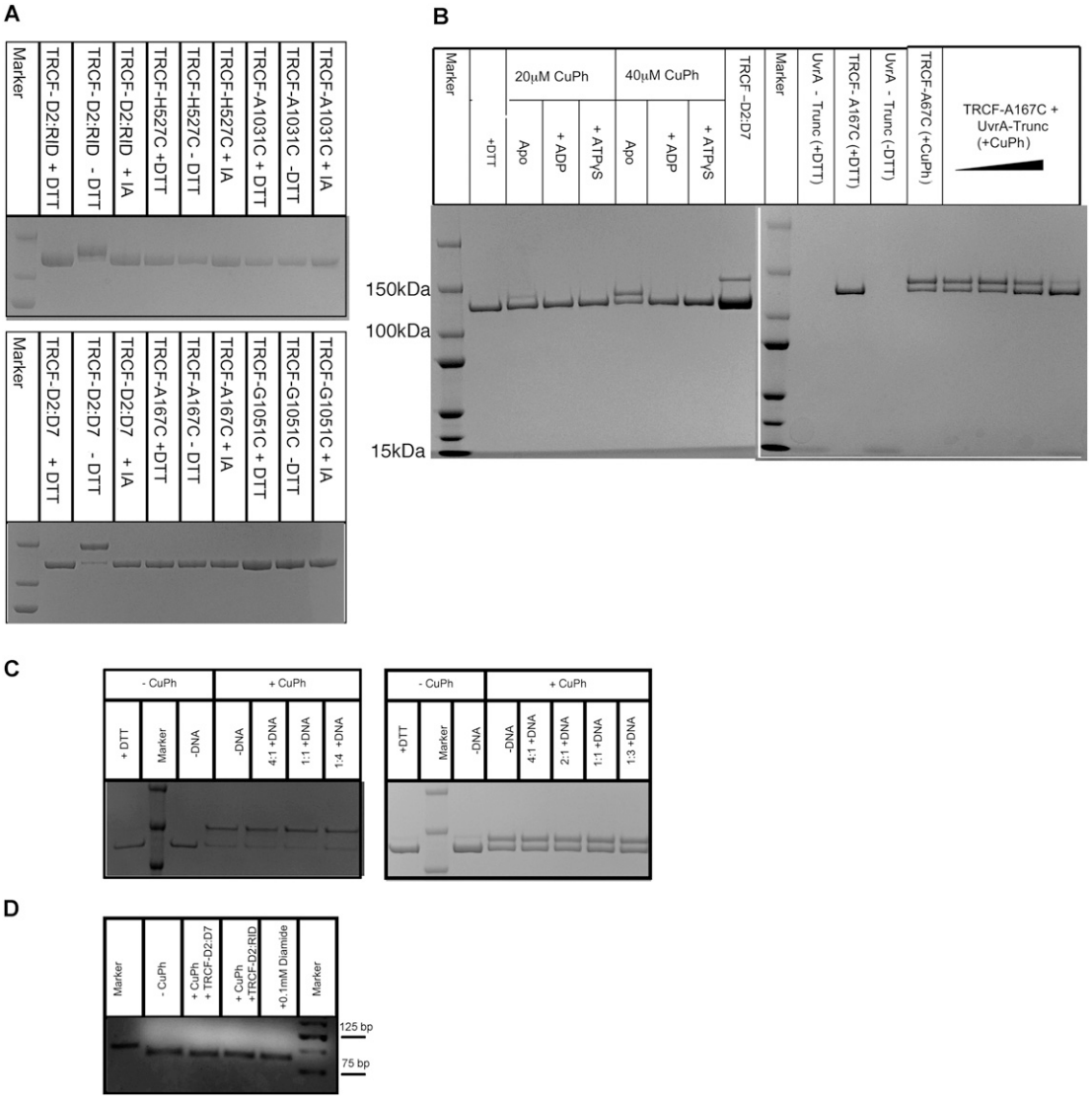

Fig. S7. Electrophoretic analysis of TRCF variants. (*A*) SDS/PAGE of the purified double mutants TRCF-D2:RID and TRCF-D2:D7 and single cysteine mutants in the presence and absence of the reducing agent DTT and the alkylating agent iodoacetamide (IA). (*B*) SDS/PAGE of TRCF-A167C cross-linking reactions in the presence of Cu(II) (1, 10) phenanthroline (CuPh) and nucleotides ADP and ATPγS (*Left*) and various concentrations of weakly staining UvrA-Trunc (*Right*). (*C*) SDS/PAGE of TRCF Cys variants, TRCF-D2:D7 (*Left*) and TRCF-D2:RID (*Right*), oxidized in the presence of CuPh and increasing concentrations of dsDNA. (*D*) Agarose electrophoresis of dsDNA incubated with CuPh (and alternative oxidizing agent diamide) in the absence/presence of TRCF variants.

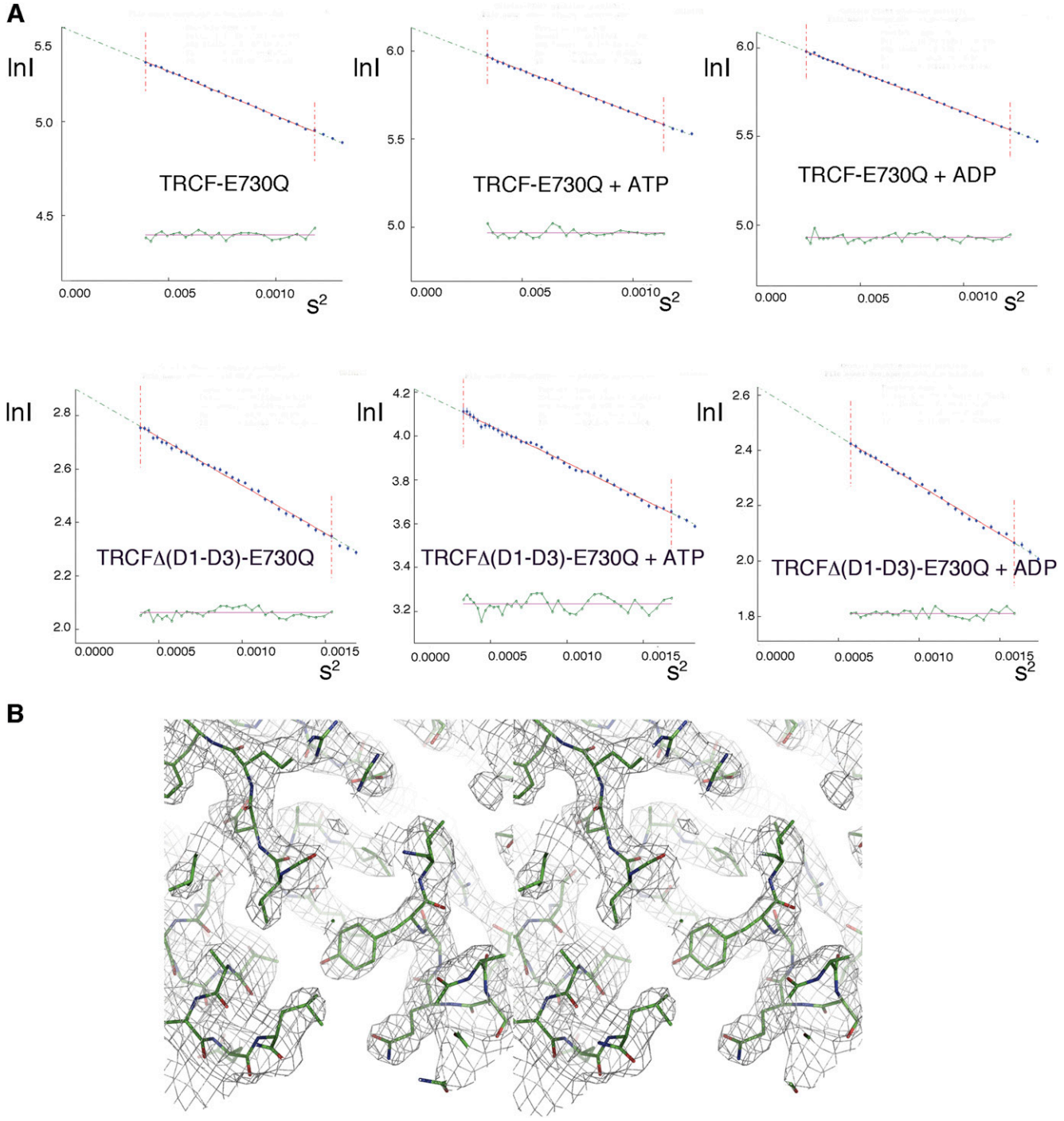

Fig. S8. Guinier analysis and electron density map. (*A*) Guinier plots of SAXS data. Graphical representation of the residuals is shown in light green. (*B*) Stereogram with a representative section of the sigmaA-validated $2|F_o| - |F_c|$ electron density map in the region of the TRCF/UvrA interface. Atomic model is shown in stick representation. The electron density map is contoured at 1.4σ.

Table S1. X-ray intensity and refinement statistics for the *E. coli* TRCF–Trunc/UvrA–Trunc complex

	TRCF-Trunc/UvrA-Trunc	
Intensity statistics	Dataset 1	Dataset 2
Space group	$P6_222$	$P6_222$
Cell dimensions		
a, b, c (Å)	119.1, 119.1, 234.2	119.2, 119.2, 234.3
α, β, γ (°)	90.00, 90.00, 120.00	90.00, 90.00, 120.00
Resolution (Å)	30.0–3.0 (3.1–3.0)*	30.0–2.8 (2.9–2.8)*
No. of reflections	20,398	24,835
R_{merge}	10.8 (64.2)*	7.5 (60.4)*
I/σI	31(2)*	26 (1.7)*
Completeness (%)	99.9 (98.3)*	99.5 (96.0)*
Redundancy	22 (12.4)*	6.4 (4.8)*
Refinement statistics		
Resolution (Å)	30.0–2.8	
No. of reflections (test set)	24,708 (1,240; random 5%)	
R_{work}/R_{free}	23.8/28.2 (41.2/49.2)*	
Cross-validated maximum-likelihood coordinate error (Å)	0.92	
No. of atoms	3,143	
Protein	3,143	
Ligand/ion	—	
Water	—	
B-factors (Å^2)		
Protein, isotropic-equivalent	93	
Ligand/ion	—	
Water	—	
rms deviations		
Bond lengths (Å)	0.008	
Bond angles (°)	1.360	

*Values in parentheses are for highest-resolution shell.

Table S2. SAXS experimental and calculated radii of gyration R_g and maximum intramolecular distance D_{max} for TRCF-E730Q and TRCFΔ(D1-D3)E730Q

	PDB ID 2EYQ	TRCF-E730Q	TRCF-E730Q+ATP	TRCF-E730Q+ADP
$R_{g,\ Experimental,\ Guinier}$ (Å)	—	37.6 ± 0.2	38.1 ± 0.3	36.8 ± 0.1
$R_{g,\ Experimental,\ real\text{-}space}$ (Å)	—	37.1 ± 0.1	38.2 ± 0.1	36.6 ± 0.1
$R_{g,\ Calculated}$ (Å)	35.8	—	—	—
$D_{max,\ Experimental}$ (Å)	—	124 ± 5	140 ± 5	126 ± 5
$D_{max,\ Calculated}$ (Å)	113	—		
	PDB ID 2EYQ Δ(D1-D3)	TRCFΔ(D1-D3) E730Q	TRCFΔ(D1-D3) E730Q + ATP	TRCFΔ(D1-D3) E730Q + ADP
$R_{g,\ Experimental,\ Guinier}$ (Å)	—	32.9 ± 0.2	31.8 ± 0.2	32.6 ± 0.2
$R_{g,\ Experimental,\ real\text{-}space}$ (Å)	—	34.1 ± 0.1	32.9 ± 0.1	33.3 ± 0.1
$R_{g,\ Calculated}$ (Å)	31.0	—	—	—
$D_{max,\ Experimental}$ (Å)	—	113 ± 5	116 ± 5	115 ± 5
$D_{max,\ Calculated}$ (Å)	102	—	—	—